Hindawi
Geofluids
Volume 2022, Article ID 2006621, 15 pages
https://doi.org/10.1155/2022/2006621

Research Article

A Nonexplosive Method for Simulating Stress Waves of Large-Scale Underground Explosions

Yuguo Ji,[1] Yuefeng Pan,[2] Shuxin Deng,[1] Fei Gao,[1] Zhangyong Zhao,[2] Tianhan Xu,[3] Songlin Yue,[3] and Zhihao Li[3]

[1]*School of Mechanical Engineering, Nanjing University of Science and Technology, Nanjing, Jiangsu 210094, China*
[2]*96911 Unit of PLA, Beijing 100032, China*
[3]*State Key Laboratory of Disaster Prevention and Mitigation of Explosion and Impact, Army Engineering University of PLA, Nanjing, Jiangsu 210007, China*

Correspondence should be addressed to Shuxin Deng; dsx@njust.edu.cn

Received 19 February 2022; Revised 17 June 2022; Accepted 4 July 2022; Published 30 July 2022

Academic Editor: Guang-Liang Feng

In the large-scale underground explosion, the dynamic mechanical behavior of deep rock mass under the coupled loading of the high in situ stress and the explosive stress wave is difficult to study. And the coupled loading of the in situ stress and the stress waves of large-scale underground explosions are hard to simulate. Based on this problem, an experimental device was developed, and a nonexplosive method for simulating stress waves of large-scale underground explosions was presented by us. In the experimental device, the impact energy is provided by the high-pressure gas in the air chamber, the stress wave is generated by the impact of the piston, and the waveform of the stress wave is adjusted by the composite pulse shaper. The adjusted stress wave can be transmitted to the container, where the coupled loading of the stress wave and the confining stress can be realized. The stress wave that corresponded to the real explosion is obtained by the developed device, and the function of the composite pulse shaper for adjusting the waveform is verified in the experiments by using a variety of mediums for wave adjustment. The experimental and calculation results showed that the stress wave corresponding to underground explosion at kilotons of equivalent on rock mass at great depth can be simulated by the experimental device, and the simulated explosion equivalent and buried depth can be adjusted by controlling the experimental conditions.

1. Introduction

When underground explosion occurs, the explosive shock wave will impact the nearby rock heavily [1], and the cavity zone, the crushing zone, the radial crack zone, and the elastic zone are formed [2], as shown in Figure 1. For the rock mass at a great depth, the rock has been being loaded by the in situ stress for a long time [3, 4]; therefore, the rock is loaded by the explosive stress wave and the in situ stress when the explosion occurs.

The high in situ stress can have an obvious influence to explosion so that the range of the cavity zone, the crushing zone, and the radial crack zone [5–7] can be changed. As for the elastic zone, before the stress wave reaches, a large amount of strain energy has been accumulated because of the high in situ stress, and the energy accumulation is more severe in surrounding rock of the tunnel settled in the elastic zone [8, 9]. When the explosion at the scale of kilotons TNT equivalent occurs, the stress wave reaches the elastic zone is with a lower stress peak but long positive pressure time. Therefore, the stress wave is with considerable energy and can break the weak interface of the rock mass, release the strain energy in the rock mass, induce the large irreversible deformation, rockburst of surrounding rock, and even cause engineering earthquake [10–13]. Thus, for the prevention and control of hazards induced by large-scale underground explosions, it is of great significance to study the dynamic mechanical behavior of rock mass under the coupled loading of high in situ stress and the explosive stress wave. The crushing zone cannot be selected as the study object because the rock is crushed completely and the crushing zone is relative small. So the rock cracks because of the coupled

loading of the stress wave, and the in situ stress should be studied in the radial crack zone and the elastic zone. However, it is very difficult to carry out the explosion test of kilotons TNT equivalent to study this problem because of the large damage scale, expensive cost, and the high possibility of disaster under high in situ stress. Besides, there are too many simplifications and assumptions in the numerical simulation research, so the numerical calculation results do not completely correspond to the field engineering [5, 12]. Therefore, it is necessary to develop an experimental device which can simulate the stress wave of large-scale underground explosion, in which device the coupled loading of the stress wave and the confining stress should be achieved.

Around experimental study of the rock failure because of the coupled loading of the stress wave and the in situ stress, many scholars have carried out studies. Kocharyan et al. [13, 14], by using a one-dimensional block model, simulated the failure phenomenon of structural blocks under the combined action of static loads and impact loads. Wang et al. [15] presented a method for simulating stress waves at scaled distance of 100 m/kt$^{1/3}$ by a set of experiment system with tiny TNT explosive balls and carried out experiments in the plexiglass and granite. He et al. [16] carried out the simulation experiment of rockburst by rock specimens with the prefabricated tunnel, and the impact loads in the form of square waves were added on the specimen on the basis of static loading. Li et al. [17] studied the dynamic mechanical response of red sandstone with different joint angles by using SHPB. Liu et al. [18] designed a circular hole to simulate the tunnel and simulate blasting stress wave by small-scale chemical explosions.

The above experimental studies have simulated the rock failure under coupled loading of the stress wave and the static stress and have important guidance and reference value for simulating the stress wave of large-scale underground explosions. However, the impact effect to rock specimens in above studies differs heavily from the stress waves of large-scale underground explosions. On one hand, the waveform characteristics of impact load such as peak value and positive pressure time are still quite different from that of the stress waves in large-scale underground explosion. On another hand, the stress wave in the above experimental study cannot couple well with the confining stress, and the static and dynamic loads on the loading boundary of the model are still not settled properly.

In addition, in the experimental study of underwater blast-resistant structures, many devices have been developed to impose blast-like pressures and impulses using nonexplosive techniques [19–21]. By using nonexplosive techniques, the strong dynamic load is generated to simulate the shock wave at the near zone of air explosion and underwater explosion [20–23]. The stress peak in the above experimental devices ranges from tens to hundreds MPa, the positive pressure time of the stress wave ranges from tens to hundreds of microseconds, and the rising pressure time is several microseconds. Therefore, the characteristics of the stress wave produced by the existing experimental devices are quite different from that of the explosive stress wave of kilotons of TNT equivalent. Also, the coupled loading of the stress wave and the confining stress is also not considered in these devices. Therefore, we developed a set of experimental device that can simulate the stress waves of large-scale underground explosions. The stress wave is generated by the impact of the steel projectile, the confining stress and the stress wave are loaded and propagated in the container, and waveform is adjusted by the impact energy and the composite pulse shaper. The results show that the stress waves generated in the experimental device are similar to the stress waves of large-scale underground explosions.

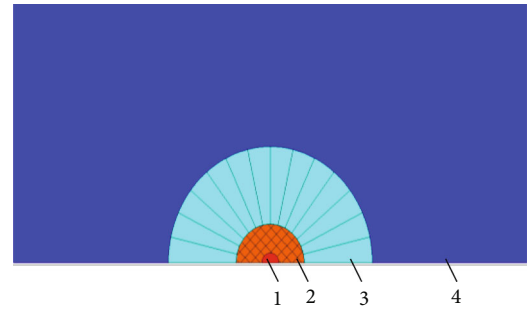

Figure 1: Zone division of rock damage. 1-cavity zone; 2-crusing zone; 3-radical crack zone; 4 elastic zone.

2. Stress Wave Analysis of Underground Explosions

A large number of measured data at large scale underground explosions of hard rock shows that, when it is outside the crushing zone, the stress wave generated by underground explosion at the scale of kilotons TNT equivalent is a half sine wave [24, 25]. The wave front can be regarded as the surface of peak particle velocity, so the expression of stress value σ_r of stress wave is [26]:

$$\sigma_r = \rho C_p v_t, \tag{1}$$

where ρ is the density of the rock; C_p is the longitudinal wave of rock; v_t is the particle velocity in the real explosion when the explosion distance is r, m/s, r is the real explosion distance to center, m, and the equation (Eq.) of particle velocity v_t is [25, 27]

$$v_t = A(\bar{r})^{-n} \sin\left(\frac{\pi t}{\tau}\right) \quad 0 \le t \le \tau, \tag{2}$$

where $\bar{r} = r/Q^{1/3}$ is the scaled distance, m/kt$^{1/3}$; Q is explosive equivalent, kiloton (kt); A and n are coefficients determined experimentally, and τ is the positive pressure time of the stress wave, ms; t is the time of the stress wave, ms.

When Eq. (2) is taken into Eq. (1), the variation relationship between the value of stress σ_a with time t is written as follows [25, 27]:

$$\sigma_a = A\rho C_p \left(\frac{r}{Q^{1/3}}\right)^{-n} \sin\left(\frac{\pi t}{\tau}\right). \tag{3}$$

As shown in Figure 2, the main parameters of half sine waves are positive pressure time and the peak value of stress waves. When $t = \tau/2$, the particle velocity at wave front is the largest, and the stress peak is written as follows:

$$\sigma_r = A\rho C_p(\bar{r})^{-n}. \tag{4}$$

The expression of the positive pressure time outside of the crushing zone can be written as

$$\tau = BQ^{1/3}(\bar{r})^m, \tag{5}$$

where B and m are the parameters determined by the tests. $\bar{r}$ in Eq. (4) and Eq. (5) is the scaled distance outside the crushing zone, and the equation of the crushing zone can be written as

$$\left.\begin{aligned} \bar{r}_{\text{crush}} &= \left(\frac{E}{3\sigma_*}\right)^{1/3}\bar{r}_{\text{cav}} \\ \bar{r}_{\text{cav}} &= \frac{r_{\text{cav}}}{Q^{1/3}} \\ r_{\text{cav}} &= \frac{\beta Q^{1/3}}{\left(\rho C_p^2\sigma_*^2\right)^{1/9}} \end{aligned}\right\}. \tag{6}$$

β is coefficient; σ_* is ultimate compression stress limit of rock mass, Pa; E is elastic modulus of the rock mass, Pa, and there is a relationship between E and the longitudinal wave velocity C_p under the condition of limited compression: $\rho C_p^2 = E(1-\upsilon)/(1+\upsilon)(1-2\upsilon)$.

The stress peak and the positive pressure time of stress wave at any explosion equivalent outside the crushing zone can be calculated by the above equations.

3. Similarity between the Model Tests and the Field Engineering

A good corresponding relationship between the action of the stress waves was generated by the experimental device to the model and the action of the explosive stress waves of the real underground explosion to the rock at great depth.

Therefore, the similarity relationship between simulated stress waves and the stress waves of real underground explosions should be established. And so do the similarity relationship between the confining stress of the model and high in situ stress at great depth. The main similarity parameters of the model contain similarity ratio of geometry ξ_H, similarity ratio of wave velocity ξ_C, similarity ratio of bulk density ξ_γ, similarity ratio of stress ξ_σ, similarity ratio of material density ξ_ρ, the similarity ratio of elastic modulus ξ_E, and similarity ratio of time ξ_T. The similarity relationships are as follows [28, 29]:

$$\xi_\sigma = \xi_E = \xi_H\xi_\gamma, \xi_H = \frac{D_f}{D_m}, \xi_\gamma = \frac{\psi_f}{\psi_m}, \xi_\rho = \xi_\gamma, \tag{7}$$

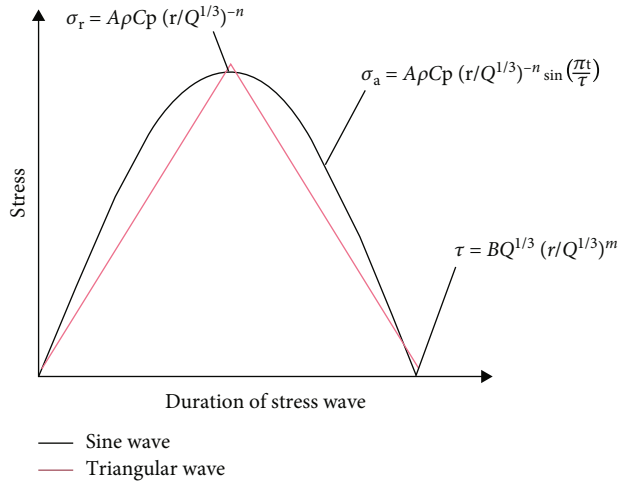

Figure 2: Waveform of the stress curve outside the crushing zone.

where D is the geometric dimension; ψ is the bulk density; the subscript "f" represents the prototype and the subscript "m" represents the model.

In the similar relationship of time in the wave propagation, when the elastic wave passes through the model material, the elastic wave velocity C in the model material determines the time in the wave propagation. In the study of the wave propagation in rock mass, the relationship between distance L and time t is written as follows [29]:

$$L_f = C_f t_f, \tag{8}$$

$$L_m = C_m t_m. \tag{9}$$

And then there is

$$\xi_T = \frac{\xi_H}{\xi_C}. \tag{10}$$

In general, the elastic wave velocity C in solids can be expressed as follows:

$$C = \sqrt{\frac{E_0}{\rho_0}}, \tag{11}$$

where E_0 is elastic modulus of the geological material, and ρ_0 is density of the geological material.

And then there is

$$\xi_C = \sqrt{\frac{\xi_E}{\xi_\rho}} = \sqrt{\frac{\xi_\sigma}{\xi_\rho}} = \sqrt{\frac{\xi_\rho\xi_H}{\xi_\rho}} = \sqrt{\xi_H}. \tag{12}$$

Based on Eqs. (11) and (12), it can be concluded that

$$\xi_T = \sqrt{\xi_H}. \tag{13}$$

While following the above similarity relationship, the feasibility and convenience of experiment should be

considered when simulating explosive stress waves of large-scale underground explosions, and the similarity ratio should be determined reasonably between the real geomechanical parameters of underground explosion and the geomechanical model material parameters. Many large-scale underground explosions have been carried out at Novaya Zemlya test site, and the rock physical and mechanical parameters that can be used to describe its geological properties are shown in Table 1. The cylindrical plexiglass, with a density of 1780 kg/m^3, a wave velocity of 1600 m/s, a diameter of 300 mm, and a thickness of 200 mm, is used as the experimental model.

In order to obtain as much experimental data as possible in the experimental device, no model is placed in the experiment, so that many sensors can be arranged. However, the parameters of the PMMA model are still used to calculate the similarity ratio, which can provide a basis for the loading capacity of the device to simulate large-scale underground explosion. According to the above parameters, the similarity ratio of bulk density ξ_γ is 1.5, the similarity ratio of elastic modulus ξ_E is 81, the similarity ratio of stress ξ_σ is 81, the similarity ratio of geometry ξ_H is 54, the similarity ratio of wave velocity ξ_C is 7.35, and the time similarity ratio ξ_T is 7.35.

Based on the geomechanical parameters of the Novaya Zemlya test site and Eqs. (4) and (5), the positive pressure time and stress peak of 1 kt equivalent at the boundary of crushing zone can be calculated. According to the above calculation, in the model experiment, the corresponding positive pressure time of simulated stress wave is about 1.66 ms, and the stress peak of the simulated stress wave is about 5.39 MPa. Therefore, it can be seen that, in the experiment of simulating underground explosion, the stress peak is at the scale of MPa, and the positive pressure time is at the scale of millisecond.

Table 1: The calculation parameters of granite.

ρ /(kg/m^3)	C_p /(m/s)	σ_* /(Pa)	υ	β	B/(m)	m	n	A
2670	4800	2×10^8	0.25	9.8×10^3	1.2×10^{-5}	1.89	1.6	0.19

4. Experimental Device

4.1. Component Introduction. According to the characteristics of stress waves of large-scale underground explosions, our research group independently developed an experimental device to simulate the stress waves. As shown in Figure 3, the experimental device is mainly composed of a high-pressure gas cavity, a solenoid valve, a launch tube, a steel projectile, a composite pulse shaper, and a container. The air chamber, acceleration pipe, and container are made of high-strength steel. The gas chamber that is with a thick wall of 25 mm can hold volume of 3 L and bear the pressure of 10 MPa. The launch tube is 730 mm long and can be divided into two parts in terms of the diameter. The part with a diameter of 120 mm is 600 mm long and is used for accelerating the steel projectile. The part with a diameter of 140 mm is 120 mm long and is used for placing composite pulse shaper. With the comprehensive control of the gas pressure, working time of the solenoid valve, and the different acceleration lengths realized in the launch tube, the impact energy for generating stress wave can be adjusted. The composite pulse shaper is composed of the polytetrafluoroethylene (PTEF) plate, the pressure plate, and the medium for wave adjustment. The length of the medium for wave adjustment is 88 mm, and it has a long compression travel during the impact process of the steel projectile. The composite pulse shaper can provide different loading rates when the mediums for wave adjustment are soft, medium hard, and hard, respectively. The diameter of the wavefront is 148 mm when the stress wave reaches the container, and it will get expanded at the help of the conical cover in the container. Finally, the stress wave and the confining stress are coupled in the closed container.

4.2. Coupled Method of the Stress Wave and the Confining Stress. Deshpande et al. [20, 21] designed a simulation device of one-dimensional plane wave based on the principle of the fluid-structure interaction (FSI). The schematic of this device is shown in Figure 4. In a steel cylinder with a diameter of 45 mm, the liquid is regarded as a bilinear elastic material with only compression capacity but no tensile capacity. In the device, the stress wave was generated by the impact of the steel projectile to the Al piston, and then, the stress wave propagates to the specimen at the other end. Although the loading of the plane wave can be achieved by this device, the action area of the plane wave is limited by the area of the piston, so the size of the specimen is very limited. For solving this problem, Espinosa et al. [22] designed a diffusive-shaped pressure tube, and the schematic is shown in Figure 5. In this device, the size of the specimen is larger than the size of the piston. By adjusting the length and angle of the pressure tube, the planeness of the stress wave is adjusted, and in the meanwhile, the interference of the stress reflection on the loading process of the specimen is avoided.

In the above research, the steel projectile directly impacts the piston, and the stress waves are formed, which are transferred to the specimen through the water in the pressure tube. According to this method, based on the mechanical characteristics that the ideal fluid can only transfer pressure, the water is used to transfer the confining stress and the stress wave. Significantly, the pressure plate is designed to work for the sealing of container with other components so that the loading of the confining stress and the propagation of stress wave in container are achieved. On the outer edge of the pressure plate, a boss structure is designed, which is larger than the diameter of the flange. In the loading stage of the confining stress, the container is firstly filled with water, and then, the water is pumped into the container through the electric pressure pump. In this process, the pressure plate compresses the flange plate and creates a sealed space with the tail cover, container pipe, flange plate, and inlet valve. Therefore, a stable confining stress environment is created to simulate the high in situ stress environment of

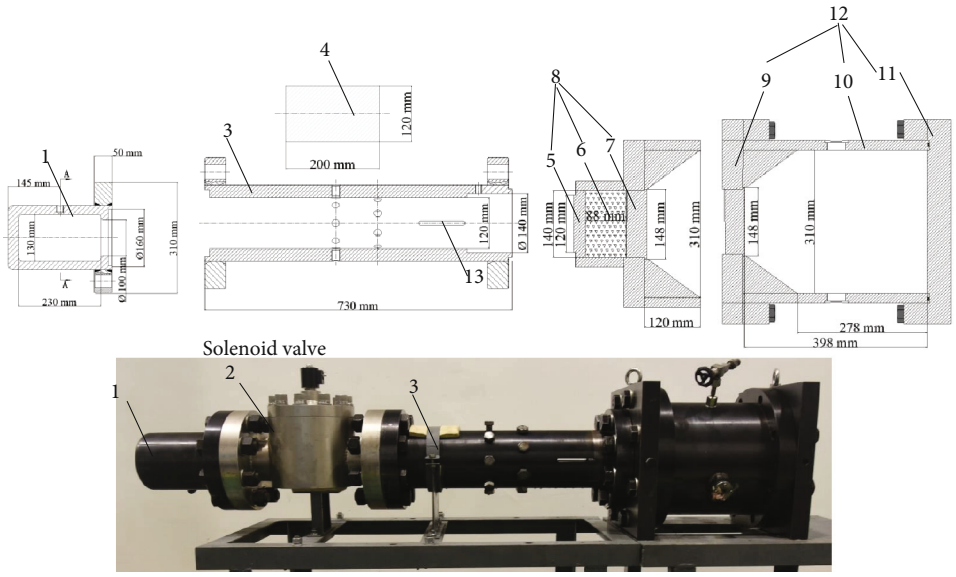

Figure 3: Schematic of the experimental device and its main components. 1-High-pressure gas chamber; 2-solenoid valve; 3-launch tube; 4-steel projectile; 5-PTEF plate; 6-the medium for wave adjustment; 7-pressure plate; 8-composite pulse shaper; 9-flange plate; 10-container tube; 11-bottom cap; 12-container; 13-observation hole of velocity of the steel projectile.

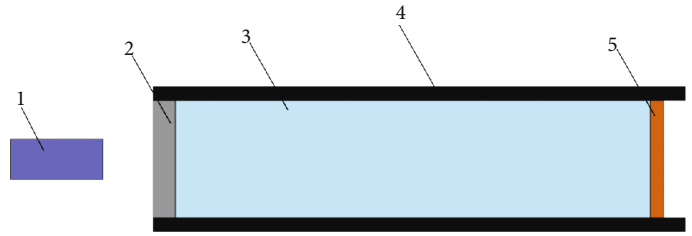

Figure 4: Schematic of the water tube experimental set-up. 1-Steel projectile; 2-Al piston; 3-water; 4-steel tube; 5-test specimen.

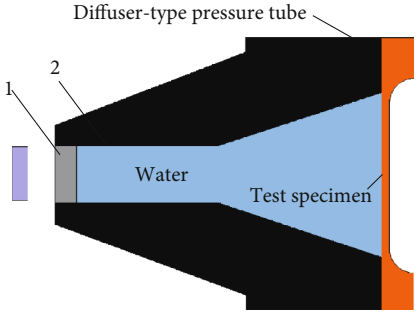

Figure 5: Schematic of water chamber with divergent diffuser. 1-Steel projectile; 2-Al piston; 3-water; 4-steel tube; 5-test specimen.

the deep rock mass, and the highest confining stress in the container can reach 20 MPa.

After the formation of confining stress in the container, the inlet valve for water of the container will be closed to keep the balance of the confining stress. As shown in Figure 6, when the steel projectile impacts the PTEF plate and compresses the buffer material, the pressure plate can freely transmit the stress wave generated by the impact energy to the container, so that the water can transmit the stress wave under the confining stress environment. Meanwhile, the boundary problem of static loading and dynamic loading is well dealt with in this device.

4.3. Formation and Adjustment Mechanism of the Stress Wave. As shown in Figure 7, the composite pulse shaper is designed to replace the fixed piston. Instead of the fixed piston [19–23], the buffer material with different bulk modulus can be used to realize the compression and rebound process to adjust the positive pressure time.

The formation process of stress wave can be divided into the following three stages. As shown in Figure 7, in the analysis of the formation of the simulated stress wave, the steel projectile and pressure plate are taken as references. In the first stage, gas runs out of the high-pressure gas cavity when the solenoid valve is opened, and the steel projectile accelerates in the launch tube. The steel projectile impacts the PTEF plate and compresses the buffer material. At this time, the stress value of the buffer material increases, but it is less than the confining stress in the container, and only the PTEF plate moves. In the second stage, the PTEF plate continues to compress the buffer material, the static state of the pressure plate is broken, the stress value of the buffer material is higher than the confining stress in the container, and the pressure plate begins to move towards the interior of the container. At this time, the PTEF

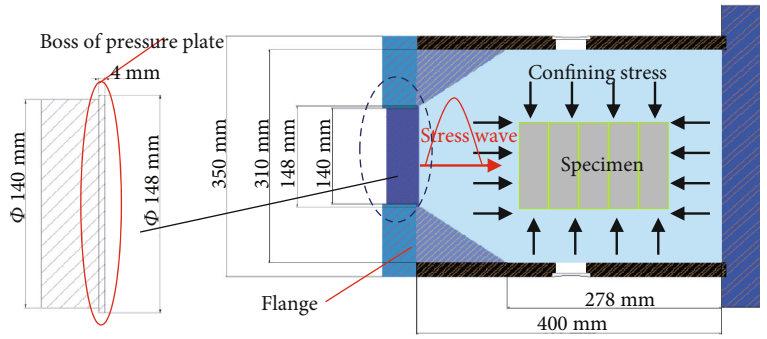

Figure 6: Schematic of confining stress and stress wave in the container.

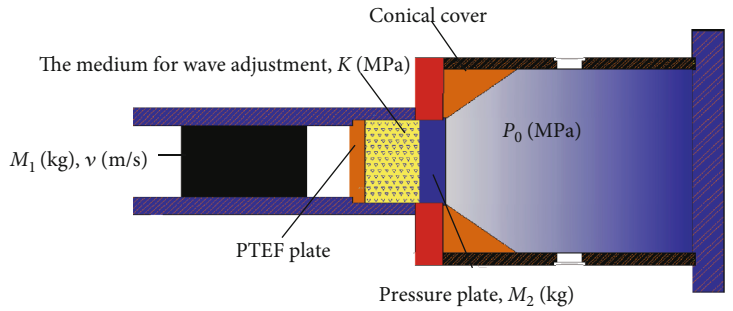

Figure 7: Formation mechanism of the stress wave in the developed experimental device.

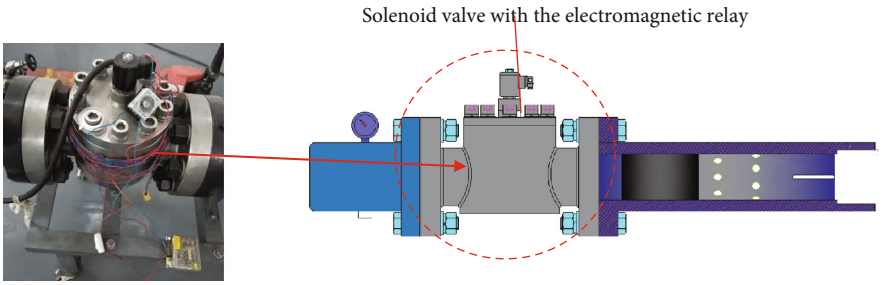

Figure 8: Experimental components of impact energy control.

plate and the pressure plate move together until the pressure plate is at a state of the largest displacement. At this time, the stress wave reaches the peak value, and this state is corresponding to the largest water compression in the container. At the third stage, the pressure plate began to rebound and finally the pressure plate is in a balanced state. And the completed processes of compression and rebounding are corresponding to the rise and drop process of the stress wave at the position of the pressure plate.

The mass of the steel projectile is M_1 (unit: kg); the displacement of the steel projectile is $u_1(t)$ (unit: m) and is a function of time t (unit: s). The mass of the pressure plate is M_2 (unit: kg); the displacement of the pressure plate is $u_2(t)$ (unit: m) and is a function of time t. The bulk modulus of the buffer medium is K (unit: MPa), the section area of the pressure plate is S (unit: m^2), the confining stress of the container is P_0 (unit: MPa), and the stress value of the container $P(t)$ (unit: MPa) at any time is a function of time t. Assuming the moment of equilibrium between the stress of the buffer material and the container is t_0, the equations of motion at the first stage are as follows [30]:

$$\begin{cases} M\ddot{u}_1(t) = -\dfrac{KSu_1(t)}{L_1}, \ 0 \le t \le t_0, \\ m\ddot{u}_2(t) = 0, \ 0 \le t \le t_0. \end{cases} \tag{14}$$

When the steel projectile impacts the PTEF plate, the initial displacement u_0 of PTEF plate and the initial velocity v_0 can be gotten, so that the velocity and displacement at t_0 can be obtained. The equations of motion of the experimental device in the second or third stage are established as follows:

$$\begin{cases} M_1\ddot{u}_1(t) = -\dfrac{KS[u_1(t) - u_2(t)]}{L_1}, \quad t_0 < t, \\ M_2\ddot{u}_2(t) = \dfrac{KS[u_1(t) - u_2(t)]}{L_1} - P(t) \cdot S, \quad t_0 < t, \end{cases} \tag{15}$$

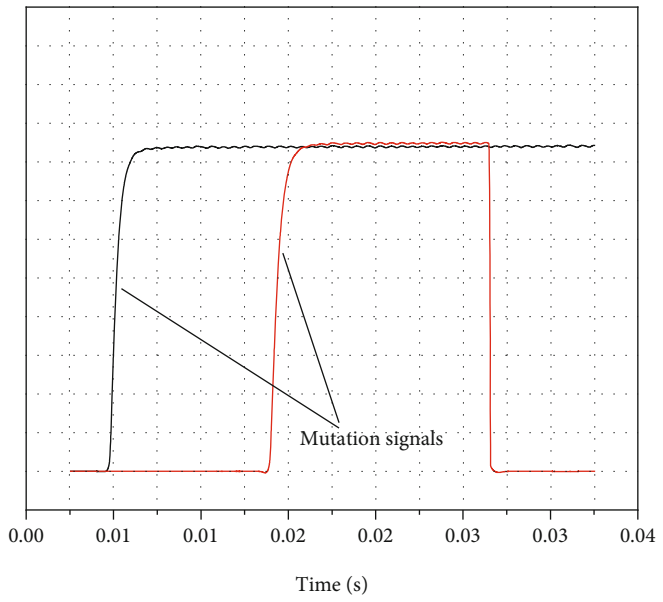

Figure 9: Laser signal of velocity observation.

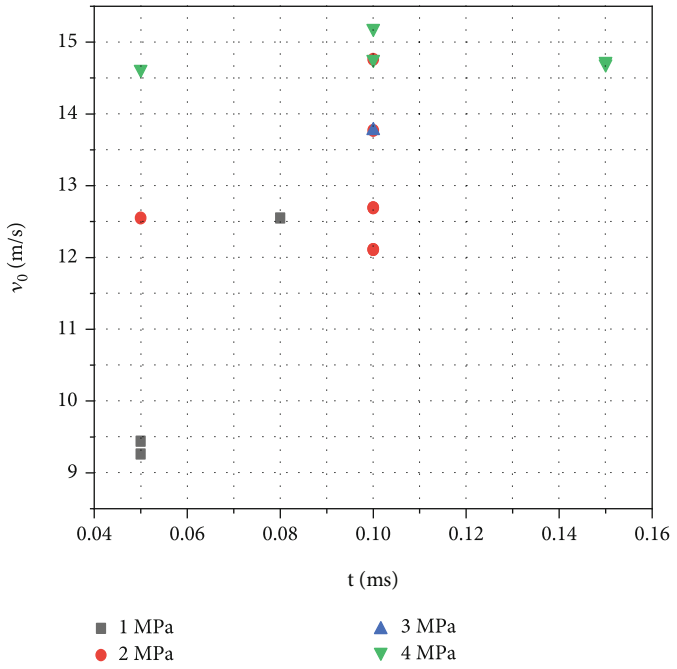

Figure 10: The steel projectile velocity under different control conditions.

Then, we can get

$$\begin{bmatrix} M_1 & 0 \\ 0 & M_2 \end{bmatrix} \begin{bmatrix} \ddot{u}_1(t) \\ \ddot{u}_2(t) \end{bmatrix} - \frac{KS}{L_1} \begin{bmatrix} -1 & 1 \\ 1 & -1 \end{bmatrix} \begin{bmatrix} u_1(t) \\ u_2(t) \end{bmatrix} + \begin{bmatrix} 0 \\ P(t) \cdot S \end{bmatrix} = 0. \tag{16}$$

The variation law of water volume with stress can be expressed as

$$P(t) = P_0 + \frac{1}{\beta_w} \left(1 - \frac{V(t)}{V_0} \right), \tag{17}$$

where V_0 is the volume of compressed water under the initial confining stress, β_w is the compression coefficient of water, $\beta_w = 5 \times 10^{-4}\ \mathrm{MPa}^{-1}$.

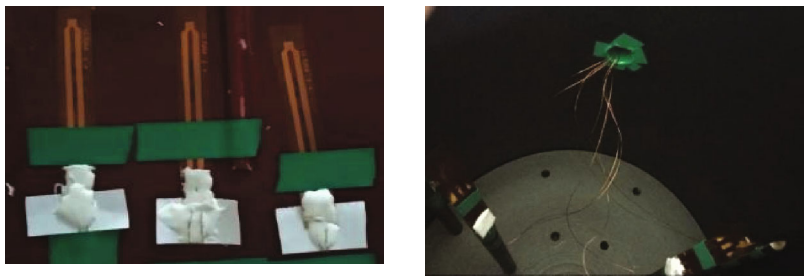

(a) PVDF gauges with waterproof glue (b) PVDF gauges fixed on the column supports

Figure 11: PVDF piezoelectric gauges.

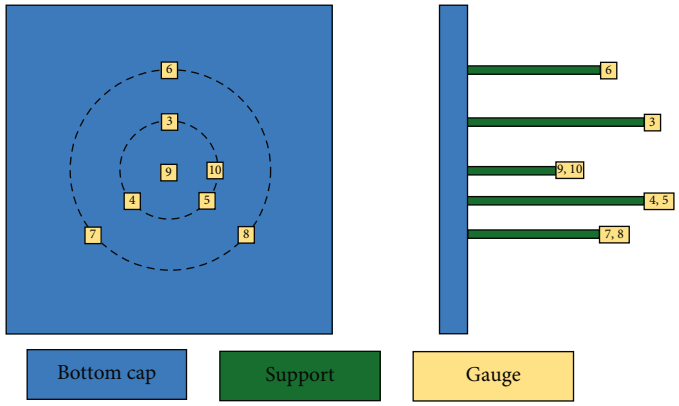

Figure 12: Positions of PVDF piezoelectric gauges.

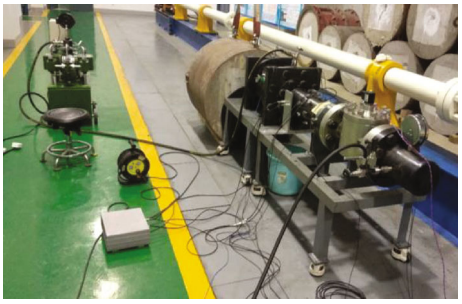

Figure 13: Completely built experimental system.

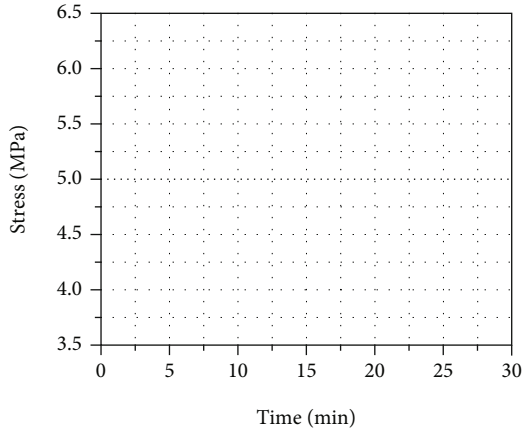

Figure 14: Observed value of confining stress.

And the water volume is calculated as follows:

$$V(t) = V_0 - u_2(t)S. \tag{18}$$

The main function of water is to transfer stress to the specimen and the container, which means its contribution to the compression is very small. So, the compression is only near the pressure plate, and the stress P around the pressure plate is

$$P = \frac{u_2(t)S}{V_0}\frac{1}{\beta} + P_0. \tag{19}$$

After the completion of the third stage, the stress wave propagates into the container. In the process of propagation, it passes through the conical cover. The cross-sectional area of the conical cover designed in the container continuously expanded to be the same as that of the container pipe. Therefore, when the stress wave passes through the conical cover, the stress wave propagates radially along the central axis of the container, and the wave front expands continuously in the form of a plane wave. According to the law of conservation of mass in fluid mechanics, it is known that

$$\oint \rho_f v_{f1} \cdot dA_{r1} = \oint \rho_f v_{f2} \cdot dA_{r2}, \tag{20}$$

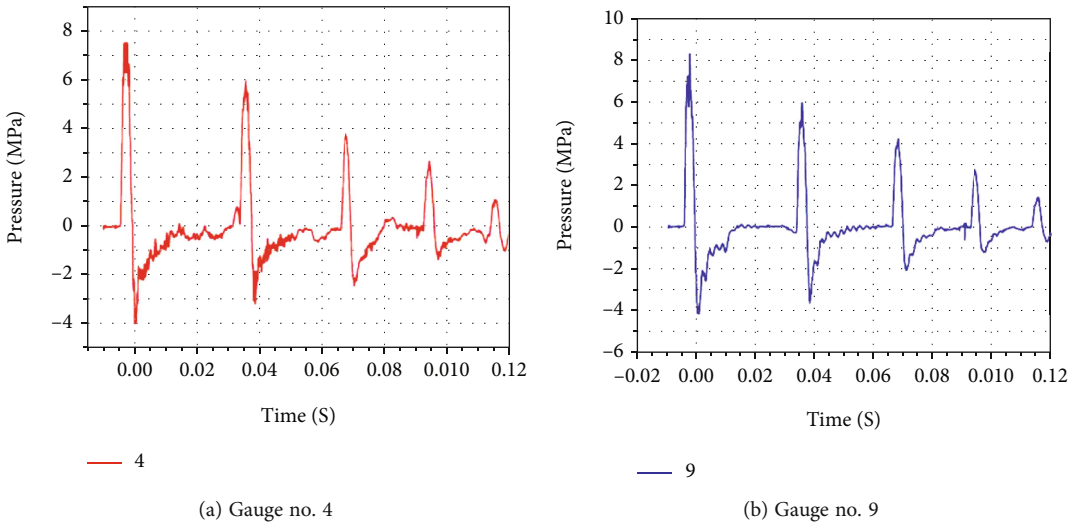

(a) Gauge no. 4 (b) Gauge no. 9

Figure 15: Stress curves of the whole experiment.

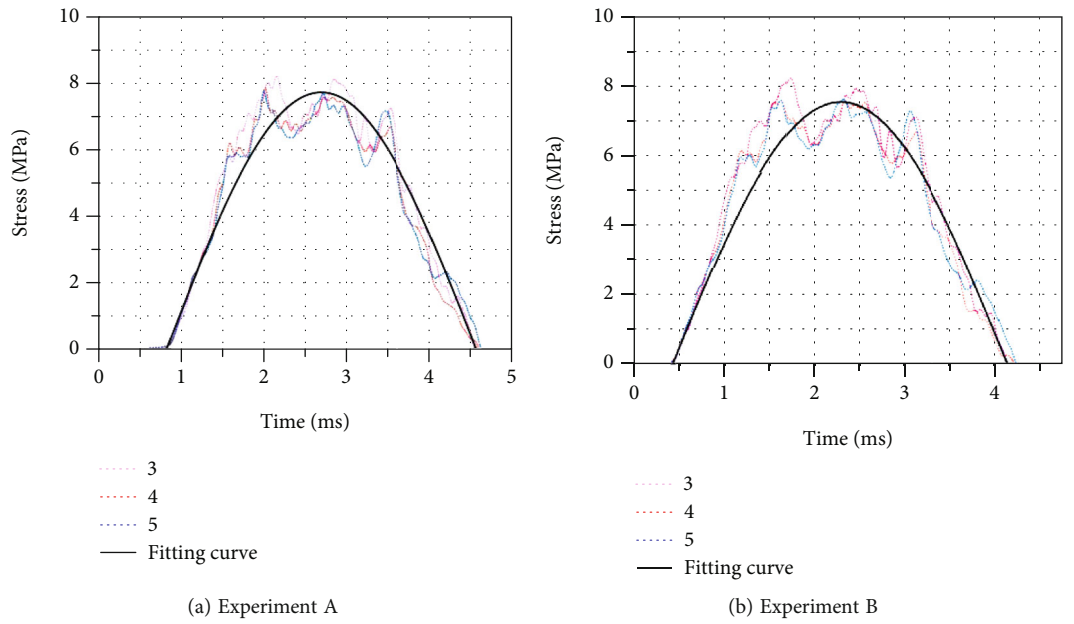

(a) Experiment A (b) Experiment B

Figure 16: Stress curves of group I.

where ρ_f is the density of fluid, kg/m^3; v_{f1} and v_{f2} are velocities of fluid at different area, and A_{r1} A_{r2} are fluid areas.

In the process of the expansion of the wave front, the velocity of the fluid on the corresponding wave front decreases. According to Eq. (1), we can know that stress peak decreases, and the positive pressure time becomes longer.

4.4. Control Methods of Impact Energy. Assuming that the friction of the steel projectile remains constant, the velocity of the steel projectile is determined by the initial driving force on the steel projectile and the acceleration process provided by the launch tube. The driving force on the steel projectile when it is accelerating in the launch tube is determined by the pressure of the gas cavity and the gassing time of the solenoid valve. The pressure of the high-pressure gas cavity is monitored by the connected pressure gauge, the working time of the solenoid valve is controlled by the electromagnetic relay shown in Figure 8, and the velocity of the steel projectile is observed by the observation window at the end of the launch tube. The method of observing the velocity is to set up two sets of laser lamps in the observation window, and when the laser is covered by the steel projectile, the signal surges. As shown in Figure 9, the length of the observation window is 8 cm, and time interval between two mutation signals is 8.9 ms; thus, it is calculated that the velocity of the steel projectile is 9.4 m/s. Figure 10 shows the steel projectile speed under different control conditions. It can be seen that the higher the initial pressure is, the

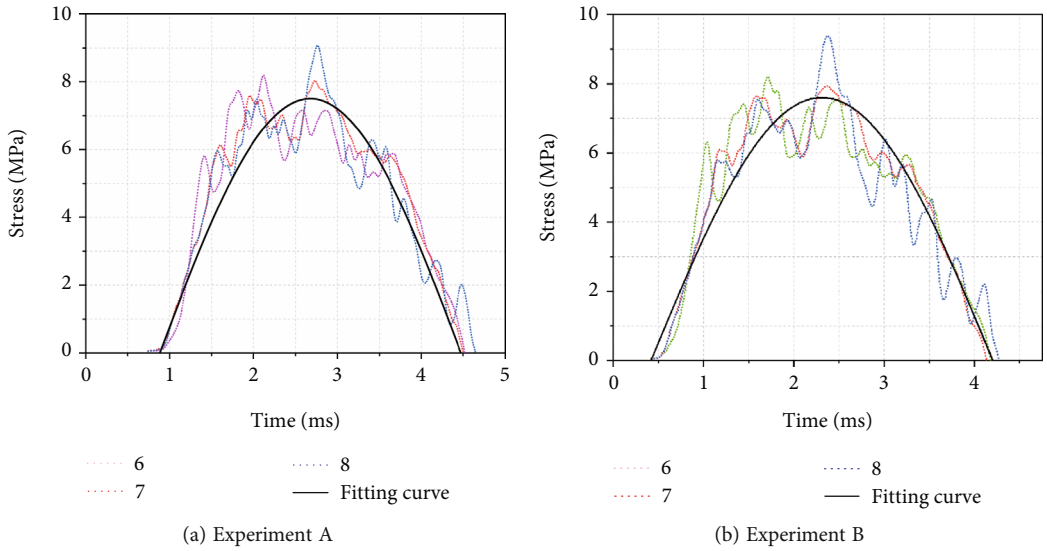

(a) Experiment A (b) Experiment B

Figure 17: Stress curves of group II.

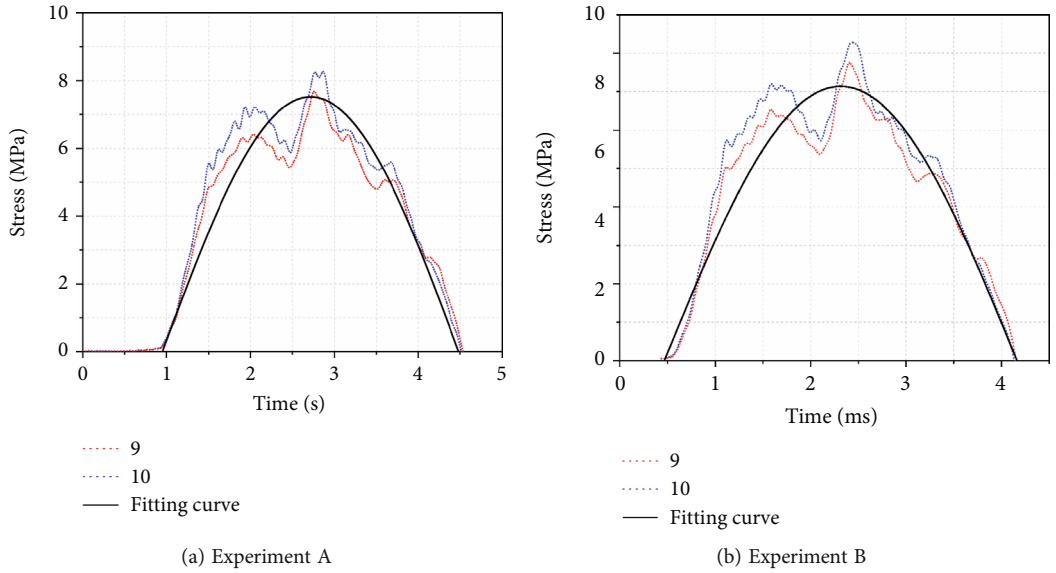

(a) Experiment A (b) Experiment B

Figure 18: Stress curves of group III.

higher the velocity of the steel projectile is when the solenoid valve has the same working time. When the working time of solenoid valve increases linearly, the change trends of velocity at different gas pressure are not consistent. When the pressure is 1 MPa, the longer the solenoid valve working time, the higher the velocity of the steel projectile. However, when the pressure values are 2 MPa and 4 MPa, the piston speed does not increase significantly when the working time of solenoid valve increases from 0.05 ms to 0.15 ms.

5. Experiments of the Stress Waves by the Developed Device

5.1. Establishment of the Whole Experimental System. The experimental device is instrumented with 8 polyvinylidene fluoride (PVDF) piezoelectric gauges [31, 32] (gauges no. 3-no. 10) to measure the stress curve. The PVDF piezoelectric gauge shown in Figure 11 is selected to measure the dynamic process of the stress wave in the container. PVDF piezoelectric gauges can be used to measure stress in an environment that is full of water. The piezoelectric effect is stable, the noise is small, the frequency response is fast, and the accuracy is high. It can directly measure the propagation process of stress waves in water.

The selected PVDF piezoelectric gauges were welded with the enameled wire, and then, the soldered dots of PVDF piezoelectric gauges were sealed with waterproof glue. The treated PVDF piezoelectric gauges were fixed on the column supports, and the column supports were fixed on the bottom cap. The relative positions of these column supports are

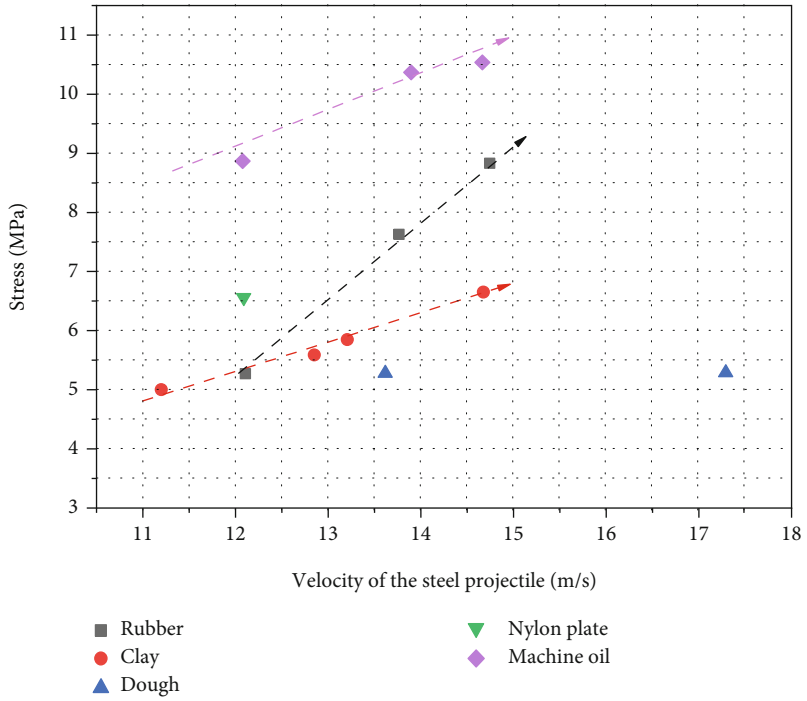

Figure 19: Peak value of stress waves in different experimental conditions.

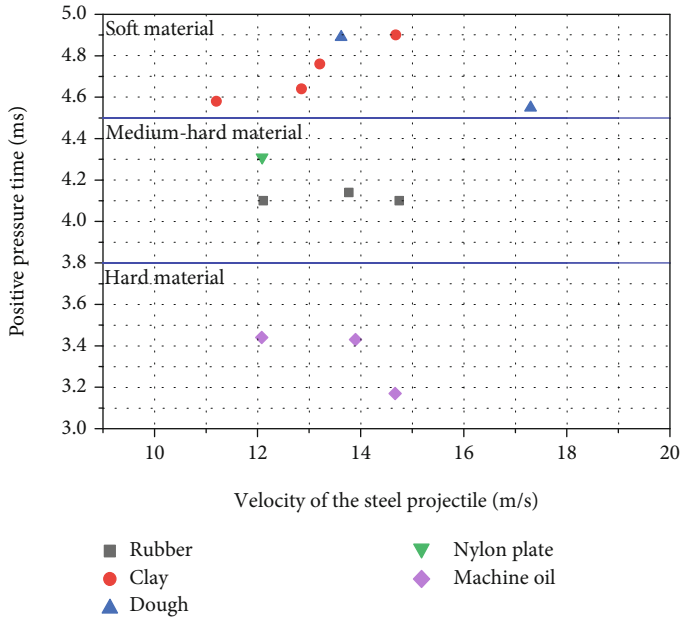

Figure 20: Positive pressure time of stress waves in different experimental conditions.

shown in Figure 12. The gauge no. 9 was set at the center, and other gauges were distributed at the concentric circles with a radius of 6.5 cm and 13.5 cm, respectively. Gauges with the same height can be used to verify whether the stress waves generated in the water propagate in the form of the plane wave. After the gauges were fixed, these enameled wires were fixed in the interior of the container and then extends out of the container tube. The stretched enameled wires were connected with the data acquisition instrument through the low resistance wire, the data acquisition instrument was connected with the charge amplifier, and the charge amplifier was connected with the data processing terminal. So far, the stress test system was built. Besides, a laser measurement system for measuring the velocity of the steel projectile was added to the experimental system for observing the instant velocity of the steel projectile when it impacts

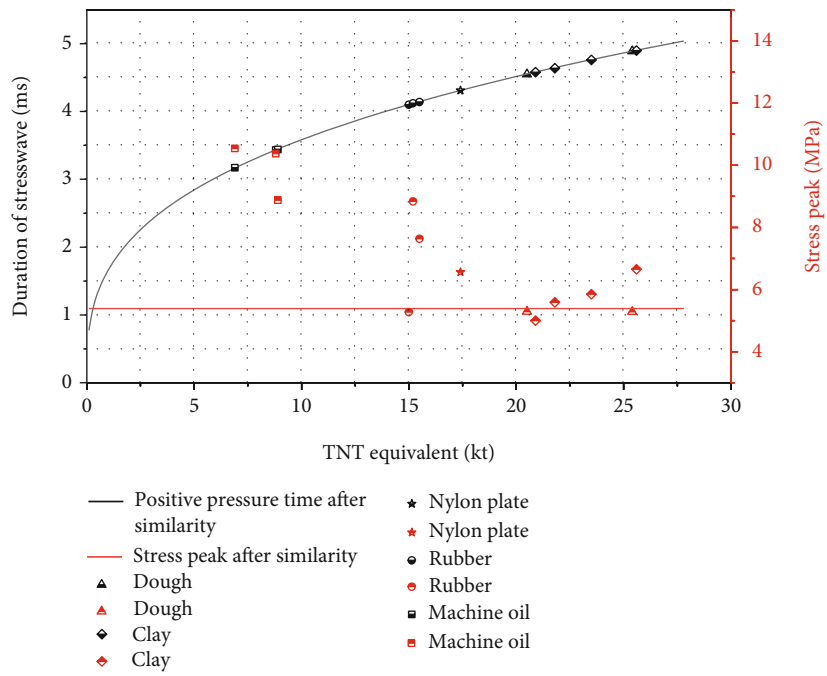

Figure 21: The positive pressure time and stress peak of experiments and large-scale underground explosions. The black color represents the positive pressure time, and the red color represents the stress peak.

Table 2: Experimental conditions.

No.	The buffer material	Velocities of the steel projectile (m/s)	The confining stress (MPa)
1	Machine oil	12.09	2
2	Machine oil	13.9	2
3	Machine oil	14.67	2
4	Rubber	12.11	2
5	Rubber	13.77	2
6	Rubber	14.75	2
7	Nylon plate	12.09	2
8	Clay	11.2	3
9	Clay	12.86	5
10	Clay	13.21	5
11	Clay	14.68	5
12	Dough	13.62	5
13	Dough	17.3	5

the PTEF plate. To avoid suffering large displacement of the device, a damping block was added behind the container. The whole experimental system is shown in Figure 13.

5.2. Verification of Stress Waveform. Two experiments under the same working condition were carried out, named as experiment A and experiment B, respectively. In the loading of static stress, the confining stress in the container was set as 5 MPa. Because the PVDF gauge is at a high-frequency response, it cannot acquire the loading process of confining stress in the container. On this account, the external pressure gauge on the container is used to observe the pressure of water. The recording results that are recorded every 20 s are shown in Figure 14, and the overall recording time is 30 min. It can be seen that the confining stress keeps at 5 MPa steadily, which can prove that the designed container has good tightness and can simulate the in situ stress at the depth of much more than 2000 m.

The next step of the experiment was to drive the steel projectile impacting the composite pulse shaper by gas in the high-pressure gas cavity, and the gas pressure of each experiment was 3 MPa. The solenoid valve switch is not closed until the gas runs out completely. Considering that the positive pressure time of the generated stress wave is between millisecond and second, the output frequency of the stress wave ranges from 30 Hz to10 kHz. The propagation process of the whole stress wave of each sensor is highly similar; thus, only the whole stress curves of gauge no. 4 and gauge no. 9 in one experiment are shown in Figure 15. According to the number of stress peaks acquired by the gauges, it can be judged that the steel projectile impacted the PTEF plate many times under the driving effect of gas in one experiment. Because when the steel projectile rebounds after impacting the waveform shaping components, the residual gas pressure in the gas cavity continues to drive the steel projectile to work. With the continuation of the impact, the subsequent impact interval becomes shorter, the residual kinetic energy of the steel projectile decreases, and the corresponding peak stress decreases.

In the process of impact, the stress wave is transmitted to the container through water, and the pressure in the container rises. But after the impact is completed, the container is back to the loading state of confining stress. This is consistent with the loading process of rock when the real underground explosion occurs. First, the deep rock mass is at loading state of the high in situ stress, and then, the

explosive stress wave impacts the rock mass so that the stress of the rock mass increases during the impact process. Finally, the rock is back to loading state of the high in situ stress after the impact.

The negative stress can be seen from the stress curves in Figure 15. This is also a signal generated from the piezoelectric effect, but this is not the stress signal directly generated by the impact of the steel projectile. Therefore, the negative stress in this curve cannot be used as a stress signal for the propagation process of the stress wave.

5.3. Analysis of Stress Waveform. The stress peak of the first wave is the highest, and if the specimen is set in the container, the first wave will load on the specimen first. Thus, the dynamic loading effect of the first wave on the specimen is the most important. Therefore, the stress curve of the first stress wave of each gauge in each experiment is obtained. Gauges no. 3, 4, and 5 are defined as group I; gauges no. 6, 7, and 8 as group II; and gauges no. 9 and 10 as group III. Stress curves of the experiment are fitted in the form of half-sine curves, and they are shown in Figures 16–18.

It can be seen from the stress curves of the above gauges that the overall stress waveforms and details obtained by the same group of gauges in each experiment are highly similar, which shows that the wave-making function of the experimental device is very stable. According to the stress curves of different gauges at the same height in one experiment, the moment when the stress began to rise is almost identical, and the trends of stress increase, fluctuation, and decrease are very similar. According to Figures 19–21, it can be seen that the fitting curves are in good agreement with the stress curves in experiments. Besides, the positive pressure times of the stress curves are about 3.5 ms, and the stress peaks are about 7 MPa, which is at the same level with the value of the stress waves in Section 3; therefore, the device developed by us can simulate the stress waves at the scale of kilotons explosion equivalent.

5.4. Waveform Adjustment Experiments. The positive pressure time of the stress wave is controlled by using buffer materials with different stiffness, and the peak value of stress wave is controlled by the impact velocity of the steel projectile. Therefore, several experiments were carried out to verify the above calculation results. The experimental conditions are shown in Table 2, and the positive pressure time and the peak value of stress wave under different working conditions of gauge no. 10 are shown in Figures 19 and 20.

By analyzing the data when rubber and machine oil are used as the buffer material, it can be seen that the stress peak increases with the impact velocity of the steel projectile, but the positive pressure time of the stress wave remains unchanged. Under the condition of the same velocity increment, the change of stress peak when rubber is used as the buffer material is more obvious than that of the machine oil. The same trend can also be seen in several groups of data when clay was used as the buffer material and the confining stress is 5 MPa. Combined with the experimental results of the above three buffer materials, it can be seen that the higher the impact velocity of the steel projectile, the higher the peak value of the stress wave. However, for the same material, the impact velocity of the steel projectile does not have an obvious effect on the positive pressure time of the stress wave.

Under the condition that the influence of the velocity of the steel projectile on the waveform of stress wave is clear, the analysis of the experimental results whose confining stress is 2 MPa and 5 MPa, respectively, shows that, when the clay is used as the buffer material, the difference of the positive pressure time of the stress waves in the two experiments is 0.06 ms. Thus, it can be concluded that the confining stress does not have an obvious influence on the positive pressure time.

According to the theoretical analysis in Subsection 4.3, it can be found that the stiffness of the buffer material has a significant effect on the positive pressure time of the stress wave. Among the used buffer materials in the above experiments, the clay and the rubber are with the lowest stiffness. When they are used as buffer materials, the positive pressure time of the stress wave is between 4.5 and 4.9 ms so that they can be regarded as soft materials. The compression capacity of nylon and rubber is relatively low, and the stiffness is relatively high. When they are used as buffer materials, the positive pressure time of the stress wave is between 4.1 and 4.35 ms, so that they can be regarded as medium-hard materials. The compression capacity of machine oil is the worst, and the stiffness is the highest among the above buffer materials. When it is used as buffer materials, the positive pressure time of the stress wave is between 3.15 and 3.55 ms, and it can be regarded as the hard material.

5.5. Comparative Analysis between Experiments and the Large-Scale Underground Explosions. The developed experimental device aims to simulate the stress wave of underground explosion. According to Section 3, the stress wave obtained in this experiment should have a good corresponding relationship with the stress wave of underground explosion at the Novaya Zemlya test site. It can be seen from Figures 16–18 that the waveform of stress wave obtained from the experimental device is approximately half sine wave, which corresponds to the waveform of underground large-scale explosion. In terms of calculation of stress peak and positive pressure time, the explosive stress waves outside the boundary of the fracture zone are taken as the analysis object, and the mechanical parameters describing the geological attributes under the explosion effect at Novaya Zemlya test site are taken from Table 1. Then, it is easy to calculate the positive pressure time and stress peak of the explosion according to Eqs. (4) and (5). In addition, the relevant similar ratios are also calculated in Chapter 3. Thus, the stress peak and positive pressure time of 1-27 kt explosion equivalent at the boundary of the crushing zone can be calculated and converted according to the related similarity ratios. And the calculated results and the stress wave parameters obtained through the experimental device are shown in Figure 21. The experiment results are consistent with the calculated results of large-scale underground explosions in terms of the positive pressure time. The stress peaks of experiments are generally larger than the calculated

results when the explosion equivalent is from 7 kt to 17.5 kt. But the stress peaks are relative consistent when the clay and the dough are set as the pulse shaper medium. Based on the above analysis, according to the working conditions corresponding to the experimental results and the comparison between the experimental results and the calculated results, it can be concluded that the developed devices can be used to simulate stress waves of large-scale underground explosions.

6. Conclusions

Based on the developed experimental device, a nonexplosive method for simulating stress waves of large-scale underground explosions is presented in this paper. The coupled loading of the confining stress and the stress wave is realized effectively. The formation mechanism of simulated stress wave is analyzed, the simulated experiments of stress wave in water under different conditions were carried out, and the main conclusions are as follows:

(1) The stress waves produced by the device are an approximate half sine wave. The positive pressure time of the stress waves is in the scale of millisecond, the stress peak is in the scale of MPa, and these parameters are corresponding to the stress waves outside the crushing zone of large-scale underground explosions. The waveform can be adjusted by changing the velocity of the steel projectile and changing the buffer material. By the above adjusting methods, stress waves of 25 kt TNT equivalent can be produced by the device. Thus, the developed device can be used for studying the dynamic mechanical behavior of rock mass under the coupled loading of high in situ stress and the stress wave of large-scale underground explosions

(2) In the container, by taking advantage of the characteristic that water can only transmit compressive stress, the boundary problem between the loading of confining stress and stress wave can be eliminated, and the coupled loading of stress wave and confining stress can be realized

Data Availability

The data used to support the findings of this study are available from the corresponding author upon request.

Conflicts of Interest

The authors declare that there is no conflicts of interest regarding the publication of this paper.

Acknowledgments

The authors acknowledge the financial support from the National Natural Science Foundation of China (Grant nos. 12002171, 51909120, 51808553, 51527810, and 51679249) and Postgraduate Research & Practice Innovation Program of Jiangsu Province (KYCX20_0312).

References

[1] G. W. Ma and X. M. An, "Numerical simulation of blasting-induced rock fractures," *International Journal of Rock Mechanics and Mining Sciences*, vol. 45, no. 6, pp. 966–975, 2008.

[2] F. V. Donzé, J. Bouchez, and S. A. Magnier, "Modeling fractures in rock blasting," *International Journal of Rock Mechanics and Mining Sciences*, vol. 34, no. 8, pp. 1153–1163, 1997.

[3] M. He, F. Ren, and D. Liu, "Rockburst mechanism research and its control," *International Journal of Mining Science and Technology*, vol. 28, no. 5, pp. 829–837, 2018.

[4] M. Wang, J. Li, L. Ma, and H. Huang, "Study on the characteristic energy factor of the deep rock mass under weak disturbance," *Rock Mechanics and Rock Engineering*, vol. 49, no. 8, pp. 3165–3173, 2016.

[5] J.-c. Yang, K.-w. Liu, X.-d. Li, and Z.-x. Liu, "Stress initialization methods for dynamic numerical simulation of rock mass with high in-situ stress," *Journal of Central South University*, vol. 27, no. 10, pp. 3149–3162, 2020.

[6] C.-l. He, J. Yang, and Q. Yu, "Laboratory study on the dynamic response of rock under blast loading with active confining pressure," *International Journal of Rock Mechanics and Mining Sciences*, vol. 102, no. 5, pp. 101–108, 2018.

[7] J. Tao, X.-G. Yang, H.-T. Li, J.-W. Zhou, G. Fan, and G.-D. Lu, "Effects of *in-situ* stresses on dynamic rock responses under blast loading," *Mechanics of Materials*, vol. 145, article 103374, 2020.

[8] L.-j. Dong, Z. Tang, X.-b. Li, Y.-c. Chen, and J.-c. Xue, "Discrimination of mining microseismic events and blasts using convolutional neural networks and original waveform," *Journal of Central South University*, vol. 27, no. 10, pp. 3078–3089, 2020.

[9] G.-L. Feng, X.-T. Feng, B.-R. Chen et al., "Characteristics of microseismicity during breakthrough in deep tunnels: case study of Jinping-II hydropower station in China," *International Journal of Geomechanics*, vol. 20, no. 2, article 04019163, 2020.

[10] G.-L. Feng, X.-T. Feng, Y.-X. Xiao et al., "Characteristic microseismicity during the development process of intermittent rockburst in a deep railway tunnel," *International Journal of Rock Mechanics and Mining Sciences*, vol. 124, article 104135, 2019.

[11] S.-x. Deng, L. Jie, J. Hai-ming, and M.-y. Wang, "Experimental and theoretical study of the fault slip events of rock masses around underground tunnels induced by external disturbances," *Engineering Geology*, vol. 233, pp. 191–199, 2018.

[12] G.-L. Feng, X.-T. Feng, B.-R. Chen, Y.-X. Xiao, and Z.-N. Zhao, "Effects of structural planes on the microseismicity associated with rockburst development processes in deep tunnels of the Jinping-II Hydropower Station, China," *Tunnelling and Underground Space Technology.*, vol. 84, pp. 273–280, 2019.

[13] G. G. Kocharyan and A. A. Spivak, "Movement of rock blocks during large-scale underground explosions: part I: experimental data," *Journal of Mining Science*, vol. 37, no. 1, pp. 64–76, 2001.

[14] G. G. Kocharyan, A. A. Spivak, and A. M. Budkov, "Movement of rock blocks during large-scale underground explosions. Part II: estimates by analytical models, numerical calculations, and comparative analysis of theoretical and experimental data," *Journal of Mining Science*, vol. 37, no. 2, pp. 149–168, 2001.

[15] Z. Wang, L. Xiao-lan, Z. Ruo-qi et al., "An experimental apparatus for spherical wave propagation in solid," *Explosion and Shock Waves*, vol. 20, no. 2, pp. 103–109, 2000.

[16] M. He, H. Xia, X. Jia, W. Gong, F. Zhao, and K. Liang, "Studies on classification, criteria and control of rockbursts," *Journal of Rock Mechanics and Geotechnical Engineering*, vol. 4, no. 2, pp. 97–114, 2012.

[17] D. Li, Z. Han, Q. Zhu, Y. Zhang, and P. G. Ranjith, "Stress wave propagation and dynamic behavior of red sandstone with single bonded planar joint at various angles," *International Journal of Rock Mechanics and Mining Sciences*, vol. 117, pp. 162–170, 2019.

[18] L. Jian-po, Z. Chang-yin, S. Ying-tao, W. Ren, L. Gang, and X. Shi-da, "Temporal-spatial evolution of acoustic emission during progressive fracture processes around tunnel triggered by blast-induced disturbances under uniaxial and biaxial compression," *Tunnelling and Underground Space Technology*, vol. 96, article 103229, 2020.

[19] P. Huson, R. J. Asaro, L. Stewart, and G. A. Hegemier, "Non-explosive methods for simulating blast loading of structures with complex geometries," *International Journal of Impact Engineering*, vol. 38, no. 7, pp. 546–557, 2011.

[20] V. Deshpande and N. Fleck, "One-dimensional response of sandwich plates to underwater shock loading," *Journal of the Mechanics and Physics of Solids*, vol. 53, no. 11, pp. 2347–2383, 2005.

[21] V. S. Deshpande, A. Heaver, and N. A. Fleck, "An underwater shock simulator," *Proceedings of the Royal Society A Mathematical Physical & Engineering Sciences*, vol. 462, no. 2067, pp. 1021–1041, 2006.

[22] H. Espinosa, S. Lee, and N. Moldovan, "A novel fluid structure interaction experiment to investigate deformation of structural elements subjected to impulsive loading," *Experimental Mechanics*, vol. 46, no. 6, pp. 805–824, 2006.

[23] F. Latourte, D. Grégoire, D. Zenkert, X. Wei, and H. D. Espinosa, "Failure mechanisms in composite panels subjected to underwater impulsive loads," *Journal of the Mechanics and Physics of Solids*, vol. 59, no. 8, pp. 1623–1646, 2011.

[24] V. V. Adushkin and A. A. Spivak, *Underground Explosions*, AVC, Washington D C, 2015.

[25] M.-y. Wang and J. Li, "Nonlinear mechanics problems in rock explosion and shock. Part III: the calculation principle of engineering seismic effects induced by underground nuclear explosion and its application," *Chinese Journal of Rock Mechanics and Engineering*, vol. 38, no. 4, pp. 695–707, 2019.

[26] T. Xu, J. Li, M. Wa, X. Xu, and W. He, "Analysis of test data of underground nuclear explosions and calculation of irreversible deformation range," *Explosion and Shock Waves*, vol. 39, no. 12, pp. 1–13, 2019.

[27] J. Li, W. Chen, S. Cun-cheng, and M.-y. Wang, "Calculation method of irreversible displacement region radius based on block hierarchical structure under large-scale underground explosion," *Explosion and Shock Waves*, vol. 38, no. 6, pp. 1271–1277, 2018.

[28] X.-x. Zhai, "Similar simulation testing study on roof strata displacement of top-coal caving face," *Chinese Journal of Rock Mechanics and Engineering*, vol. 21, no. 11, pp. 1667–1671, 2002.

[29] P.-x. Fan, M.-y. Wang, H.-z. Xing, K.-f. Jiang, and Z.-z. Li, "Time-dependent problems of deformation and failure in geo-mechanical model tests," *Chinese Journal of Rock Mechanics and Engineering*, vol. 33, no. 9, pp. 1843–1851, 2014.

[30] D. L. Landau and E. M. Lifshitz, *Theoretical Physics Course Volume One: Mechanics*, Higher Education Press, Beijing, 5th edition, 2007.

[31] H. Kawai, "The piezoelectricity of poly (vinylidene fluoride)," *Japanese Journal of Applied Physics*, vol. 8, no. 7, pp. 975-976, 1969.

[32] F. Bauer, "Method and device for polarizing ferro electric materials," 1989, US 461126006.